doi:10.1038/nature07462

LETTERS

X-ray structure of a pentameric ligand-gated ion channel in an apparently open conformation

Nicolas Bocquet[1]*, Hugues Nury[1,2]*, Marc Baaden[4], Chantal Le Poupon[1], Jean-Pierre Changeux[3], Marc Delarue[2] & Pierre-Jean Corringer[1]

Pentameric ligand-gated ion channels from the Cys-loop family mediate fast chemo-electrical transduction[1–3], but the mechanisms of ion permeation and gating of these membrane proteins remain elusive. Here we present the X-ray structure at 2.9 Å resolution of the bacterial *Gloeobacter violaceus* pentameric ligand-gated ion channel homologue[4] (GLIC) at pH 4.6 in an apparently open conformation. This cationic channel is known to be permanently activated by protons[5]. The structure is arranged as a funnel-shaped transmembrane pore widely open on the outer side and lined by hydrophobic residues. On the inner side, a 5 Å constriction matches with rings of hydrophilic residues that are likely to contribute to the ionic selectivity[6–9]. Structural comparison with ELIC, a bacterial homologue from *Erwinia chrysanthemi* solved in a presumed closed conformation[10], shows a wider pore where the narrow hydrophobic constriction found in ELIC is removed. Comparative analysis of GLIC and ELIC reveals, in concert, a rotation of each extracellular β-sandwich domain as a rigid body, interface rearrangements, and a reorganization of the transmembrane domain, involving a tilt of the M2 and M3 α-helices away from the pore axis. These data are consistent with a model of pore opening based on both quaternary twist and tertiary deformation.

Pentameric ligand-gated ion channels (pLGICs) are allosteric proteins regulating cellular excitability through the opening of an intrinsic transmembrane ion channel. Agonist binding to extracellular sites shifts a closed conformation into an open one, allowing ions to diffuse down their electrochemical gradient. Two agonist-free structures have been reported: the *Torpedo marmorata* nicotinic acetylcholine receptor (nAChR-*Tm*), solved by electron microscopy at 4 Å resolution[11,12], and the 3.3 Å ELIC X-ray structure[10]. X-ray structures of homologues of the extracellular domain (ECD) of nAChRs have also been described: the acetylcholine-binding proteins (AChBPs) co-crystallized with agonists and antagonists[13–15], and the ECD of α1-nAChR[16]. A key issue is now to understand how pLGICs open, select and translocate ions through the membrane. Most pLGICs undergo desensitization on prolonged exposure to agonist, complicating structural investigations of the transient open conformation. In contrast, GLIC is activated by protons but does not desensitize, even at proton concentrations eliciting the maximal electrophysiological response (pH 4.5)[5]. Here we present the first apparently open structure of this family, GLIC crystallized at pH 4.6.

The overall architecture of GLIC is similar to those of ELIC, the AChBPs, and nAChR-*Tm* (Fig. 1a). The five subunits are arranged in a barrel-like manner around a central symmetry axis that coincides with the ion permeation pathway (Fig. 1b). Subunits interact tightly through a 2,200 Å^2 interface containing charged residues and water molecules (Supplementary Fig. 8). The ECD of each subunit consists of a β-sandwich composed of five inner and three outer strands connected by loops (Fig. 1c). In eukaryotic pLGICs, the interface between ECDs holds the neurotransmitter-binding pocket[2,14]. The equivalent region in GLIC presents structural similarity despite a low sequence identity, and is well defined, notably the capping β9–β10 loop (loop C)[15]. The transmembrane domain (TMD) of each subunit consists of four helices (M1 to M4). M2 helices form the wall of the pore (Fig. 2a), bordered by rings of homologous residues, as previously established in nAChRs[6,17]: a charged E−2′, two polar T2′, S6′, and three hydrophobic I9′, A13′ and I16′/L17′ rings, that are close/homologous to α1-nAChR-*Tm* E−1′, T2′, S6′, L9′, V13′ and L16′/V17′ (the prime numbering starts at approximately the beginning of M2, at positions homologous to α1K242 of nAChR-*Tm*, Fig. 2c). M1 helices are kinked at P205 and form with M3 a second circle of helices interacting with M2. M4 helices are peripheral. Well-defined electron densities are observed in the grooves between M4 and both M1 and M3, close to residues labelled by hydrophobic probes on nAChR-*Tm*[18]. They were attributed to lipids that possibly contribute to holding M4 in its position (Fig. 1b, d, and Supplementary Fig. 3). The central ion permeation pathway consists of an extracellular hydrophilic vestibule more than 12 Å wide, followed by a funnel-shaped transmembrane pore (Fig. 2d). The M2 axes are tilted with respect to the pore axis, with outer hydrophobic side chains oriented towards the helix interfaces, and inner polar side chains oriented towards the pore.

A bundle of six detergent molecules (dodecyl-β-D-maltoside, DDM) obstructs the pore, with one detergent per monomer and one sitting on the five-fold axis, the sugar moiety being much less ordered than the aliphatic chains (Fig. 1b, d, Supplementary Fig. 3). The former interact extensively with the hydrophobic rings, shielding their side chains from the solvent with the polar heads pointing up, towards the vestibule, while the latter points its polar head down. To probe the influence of the detergent on the protein conformation, diffraction data have been collected with crystals grown in the presence of two DDM analogues (Supplementary Fig. 4). These detergents contain two bulky bromine atoms in their alkyl chain and could not bind all in the same position as described here (Fig. 1) without seriously disturbing the pore structure, for steric reasons. In both cases we observe that the protein conformation is unchanged (r.m.s. deviation <0.3 Å), whereas either the central detergent is not seen in the electron density (10,11-dibromoundecanoyl-β-maltoside) or the five central detergent-binding sites are only partly occupied (7,8-dibromododecyl-β-maltoside). Furthermore, we performed molecular dynamics simulations (20 ns) of the GLIC molecule in a lipid bilayer without DDM in the pore. We observe that its conformation is stable throughout the simulation (Supplementary Fig. 6).

[1]Pasteur Institute, G5 Group of Channel-Receptor, CNRS URA 2182. [2]Pasteur Institute, Unit of Structural Dynamics of Macromolecules, CNRS URA 2185. [3]Pasteur Institute, CNRS URA 2182, F75015, Paris, France. [4]Institut de Biologie Physico-Chimique, CNRS UPR 9080, 75005 Paris, France.
*These authors contributed equally to this work.

©2008 Macmillan Publishers Limited. All rights reserved

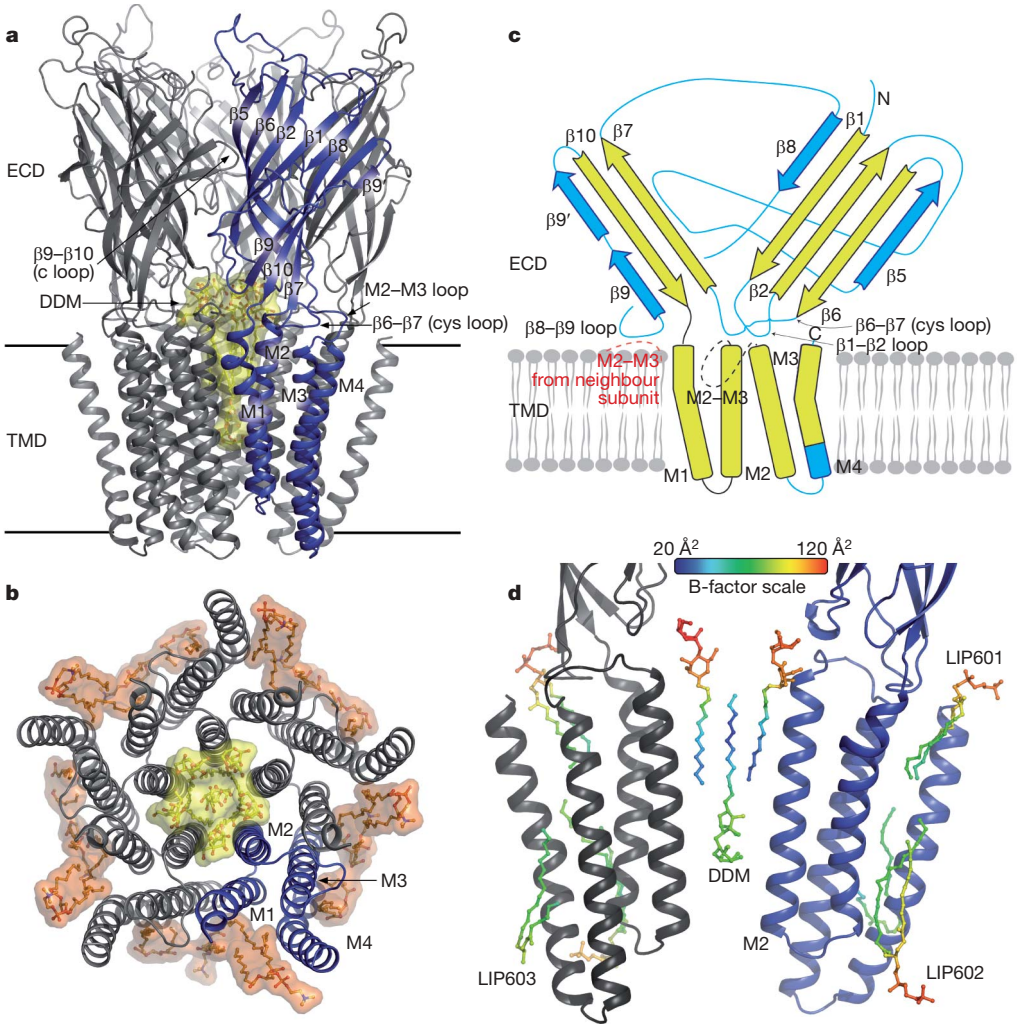

Figure 1 | GLIC structure. **a**, Ribbon representation of GLIC viewed from the plane of the membrane. DDM molecules bound in the channel are depicted as yellow sticks plus van der Waals surface. Horizontal lines represent the membrane limits. **b**, Transmembrane part of GLIC viewed from the extracellular side. The ECD is removed for clarity. Lipids are also depicted in orange. **c**, Topology of a GLIC subunit. The conserved core elements common to GLIC and ELIC are coloured in yellow. **d**, Close-up view of the TMD. Only two subunits are represented. The DDM molecules and the lipids (named LIP601/2/3) close to these subunits are coloured according to their atomic B-factor (colour scale at top).

The pore of GLIC resembles a cone with 12 Å outside and 5 Å inside diameters, sharply contrasting with that of ELIC, where outer residues L9′, A13′ and F16′ point their side chains towards the central axis, creating a 2 Å diameter hydrophobic barrier expected to prevent ion permeation (Fig. 2b). This wide opening of the pore is suggestive of an open structure. Three lines of evidence support this idea. First, GLIC was solved in the presence of a non-desensitizing agonist. Second, the GLIC pore structure is consistent with a wealth of biochemical data obtained on the open conformation of nAChRs that located the channel constriction between residues −2′ and 2′ (refs 19, 20), from measurement of cysteine accessibility[19] and channel conductance decreases following positively charged residue substitution[20]. Yet, permeability studies with organic cations suggest that this constriction is 7.5 Å wide in nAChRs[8], while it is only 5 Å wide in GLIC. Intrinsic flexibility of the side chains composing the constriction could compensate for this difference and transiently allow for accommodation of large cations. Third, molecular dynamics simulations based on the nAChR-*Tm* confirm that it corresponds to an impermeant structure, with rings 9′ and 13′ creating a hydrophobic barrier, but show that small increases (less than 2 Å) in diameter would produce a permeant channel[21,22]. The GLIC diameter is significantly wider than that of nAChR-*Tm* at these positions, further highlighting its compatibility with cation permeation.

Interestingly, mutagenesis has pointed to a key role of the −2′/2′ region in determining charge selectivity[6–9]; a ring of negatively charged residues at −1′ and an additional ring of prolines at −2′ respectively favour cationic and anionic selectivity of eukaryotic pLGICs. Thus, the −2′/2′ region was proposed to constitute the selectivity filter of the pore[7–9], an idea consistent with our structure, where the constriction is formed by the T2′ hydroxyl moieties, flanked on both sides by the S6′ hydroxyl and E−2′ carboxyl moieties. The 5 Å diameter at T2′ is too narrow to fit a fully hydrated ion, as indicated by the average distance between sodium or potassium and protein side-chain oxygen atoms (respectively 2.4 and 2.85 Å between atom centres[23]). Cation permeation would require the loss of equatorial water molecules; yet rings of polar side chains are located in the right position to transiently coordinate cations and could compensate for this loss. Regarding the pore conformation, data are thus consistent with the notion that GLIC and ELIC structures are in presumed open and closed conformations, respectively, while that of nAChR-*Tm* might be in a functionally closed but structurally nearly open conformation.

Assuming that GLIC and ELIC structures faithfully represent the open and closed forms of pLGICs embedded in a phospholipid bilayer, insight into the opening mechanism can be provided by analysing their rearrangements, even though they share only 18%

©2008 Macmillan Publishers Limited. All rights reserved

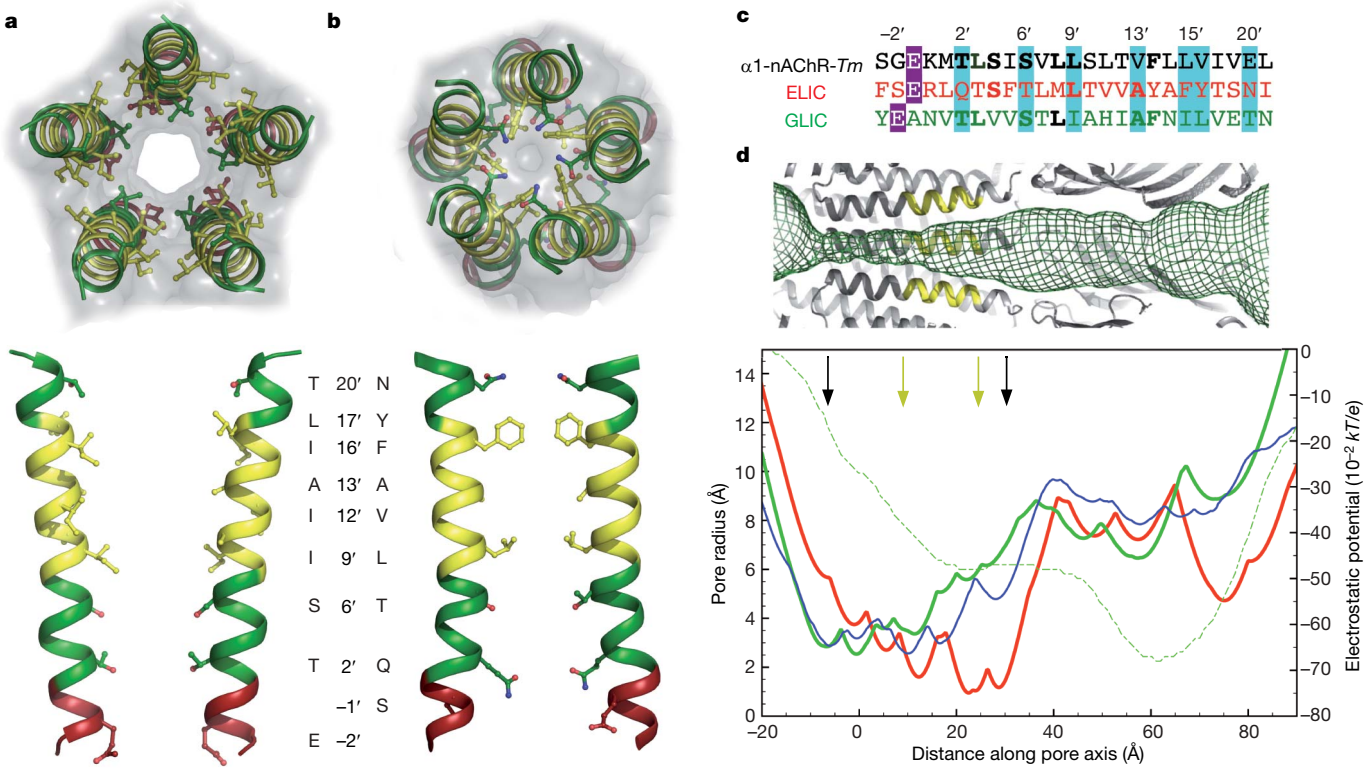

Figure 2 | GLIC and ELIC pores. **a**, Top and side view of GLIC M2 helices (top and bottom panels, respectively); helix backbones and side chains facing the pore are depicted. Hydrophobic, polar and negative residues are coloured yellow, green and red respectively. In the side view, only two subunits are shown. DDM molecules are removed for clarity. **b**, Top and side views of ELIC M2 helices. **c**, M2 sequence alignment. **d**, Pore radius for α1-nAChR-*Tm* (blue), ELIC (red) and GLIC (green) along its axis. The upper part is a mesh representation at the same scale of the GLIC channel. The electrostatic potential is represented as a dotted green line. Black and yellow arrows indicate the limits of the membrane and the hydrophobic rings, respectively.

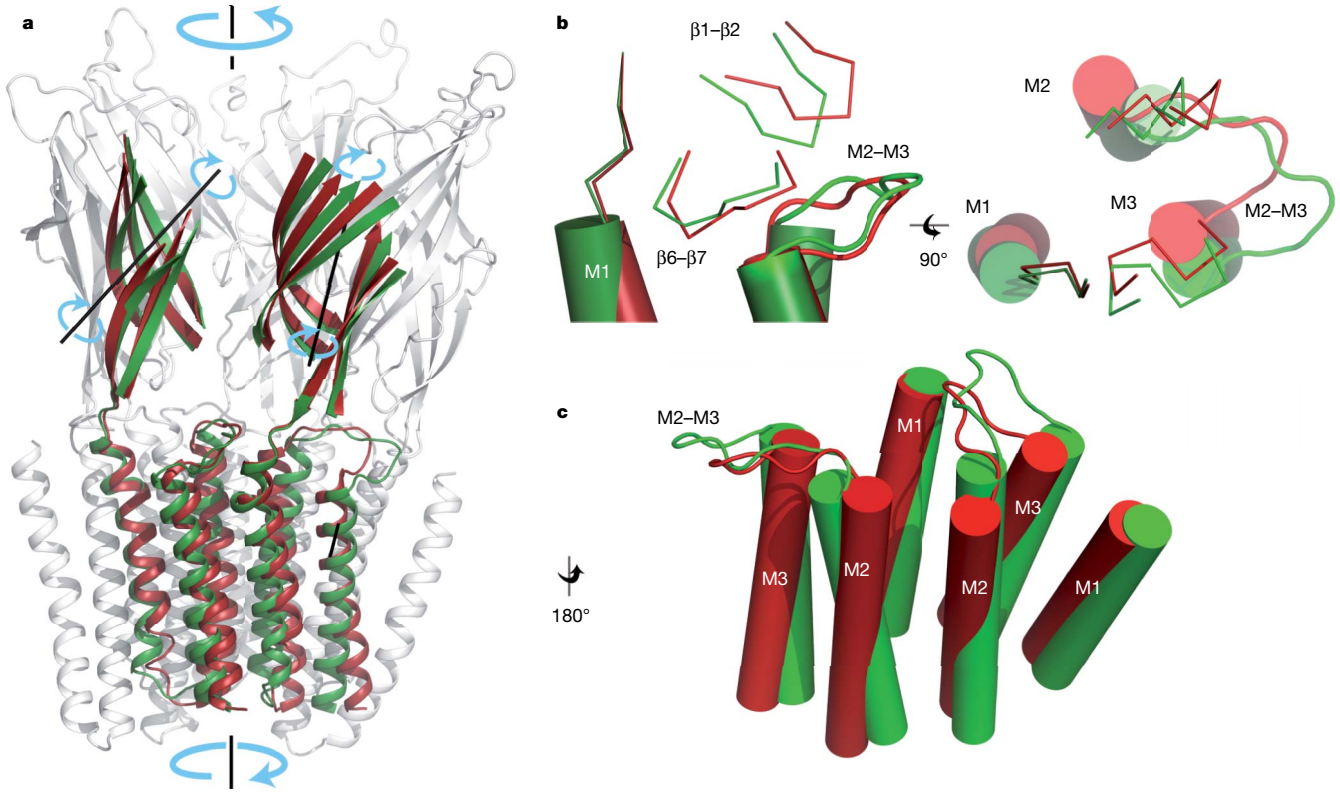

Figure 3 | Open GLIC and closed ELIC structure comparison. **a**, Side view of the structural superposition. For the two subunits in the foreground, only the common core is depicted, in green for GLIC, in red for ELIC. Other subunits are in grey. The ECD rotation axes and the twist axis are depicted. The M4 helix is omitted for clarity. **b**, Close-up view of the interface between the ECD and the TMD (side view in left panel and upper view in right panel). **c**, Close-up of transmembrane helices M1–M3 viewed from the channel.

©2008 Macmillan Publishers Limited. All rights reserved

sequence identity. Several elements can be unambiguously aligned with no gap or insertion, with identical secondary structure (Supplementary Fig. 2): helices M1, M2 and M3, and a large portion of the β-sandwich consisting of strands β1, β2, β6, β7 and β10, also well conserved in the AChBPs. These elements constitute the subunit 'common core'. Common core superimposition shows that the GLIC subunits display a quaternary twist compared to ELIC, with anti-clockwise (versus clockwise) rotation in the upper (versus lower) part of the pentamer, when viewed from the extracellular compartment (Fig. 3a). This is confirmed by normal mode analysis: the lowest frequency mode is precisely a twist mode and has by far the highest contribution (29%) to the transition (Supplementary Fig. 7a). However, we note that the first 100 lowest-frequency modes (usually the most collective ones) only explain about 50% of the transition. Other and more local movements occur: in the TMD, the outer ends of M2 and M3 of GLIC are tilted away radially from the channel axis, while the outer end of M1 is fixed. The inner ends of M1, M2 and M3 move tangentially towards the left, when viewed from the membrane (Fig. 3b). In the ECD, the core of the β-sandwich undergoes little deformation (Supplementary Table 2), but is rotated by 8° around an axis roughly perpendicular to the inner sheet of the β-sandwich (Fig. 3a), concomitant with a rearrangement of both the subunit–subunit and the ECD/TMD interfaces, regions known to contribute to neurotransmitter gating[24–27]. The latter contains the well-conserved β6–β7 and M2–M3 loops and the β1–β2 loop whose length is conserved in the pLGIC family. We observe a downward motion of the β1–β2 loop, concomitant with a displacement of the M2–M3 loop, M2 and M3 helices and β6–β7 loop towards the periphery of the molecule (Fig. 3c), thereby opening the pore.

This mechanism is different from a more local gating pathway suggested by the comparison of the conformations of the α and non-α subunits in nAChR-*Tm*[12]. It implies both a quaternary twist and tertiary deformations. Such twist to open motions, initially proposed from *ab initio* normal mode analysis of nAChRs[28], and observed for Kcsa[29], may plausibly be extended to eukaryotic pLGICs. The structural transition described here couples in an allosteric manner the opening–closing motion of the pore with distant binding sites—located at the ECD subunit interface for neurotransmitters, or within the TMD for allosteric effectors[30]—and may possibly serve as a general mechanism of signal transduction in pLGICs.

METHODS SUMMARY

GLIC was expressed as described previously[5], and solubilized/purified in 2%/0.02% DDM including an amylose affinity chromatography, two size exclusion chromatographies and thrombin cleavage of fused MBP. Crystals were grown at pH 4.6, with 15% PEG 4000, 100 mM NaOAc and 400 mM $(NH_4)SCN$ in hanging drops. Data were collected at MX beamlines of the European Synchrotron Radiation Facility, and processed with XDS and CCP4 programs (Supplementary Table 1). The spacegroup is *C*2 with one pentamer in the asymmetric unit (Supplementary Fig. 1). Molecular replacement with Phaser using the ELIC structure gave the first density maps. Refinement was conducted with Coot and Refmac, using tight NCS restraints. The final model presents a good geometry and consists of residues 6–315 for the 5 subunits plus 6 DDM and 15 partial lipid molecules, and 115 water molecules (Supplementary Fig. 3).

Received 2 June 2008; accepted 29 September 2008.
Published online 5 November 2008.

1. Corringer, P. J. & Changeux, J. P. Nicotinic acetylcholine receptors. *Scholarpedia* **3**, 3468 (2008).
2. Lester, H. A., Dibas, M. I., Dahan, D. S., Leite, J. F. & Dougherty, D. A. Cys-loop receptors: New twists and turns. *Trends Neurosci.* **6**, 329–336 (2004).
3. Sine, S. M. & Engel, A. G. Recent advances in Cys-loop receptor structure and function. *Nature* **440**, 448–455 (2006).
4. Tasneem, A., Iyer, L. M., Jakobsson, E. & Aravind, L. Identification of the prokaryotic ligand-gated ion channels and their implications for the mechanisms and origins of animal Cys-loop ion channels. *Genome Biol.* **6**, R4 (2005).
5. Bocquet, N. *et al.* A prokaryotic proton-gated ion channel from the nicotinic acetylcholine receptor family. *Nature* **445**, 116–119 (2007).
6. Imoto, K. *et al.* Rings of negatively charged amino acids determine the acetylcholine receptor channel conductance. *Nature* **335**, 645–648 (1988).
7. Imoto, K. *et al.* A ring of uncharged polar amino acids as a component of channel constriction in the nicotinic acetylcholine receptor. *FEBS Lett.* **289**, 193–200 (1991).
8. Keramidas, A., Moorhouse, A. J., Schofield, P. R. & Barry, P. H. Ligand-gated ion channels: Mechanisms underlying ion selectivity. *Prog. Biophys. Mol. Biol.* **86**, 161–204 (2004).
9. Corringer, P. J. *et al.* Mutational analysis of the charge selectivity filter of the α7 nicotinic acetylcholine receptor. *Neuron* **22**, 831–843 (1999).
10. Hilf, R. J. & Dutzler, R. X-ray structure of a prokaryotic pentameric ligand-gated ion channel. *Nature* **452**, 375–379 (2008).
11. Miyazawa, A., Fujiyoshi, Y. & Unwin, N. Structure and gating mechanism of the acetylcholine receptor pore. *Nature* **423**, 949–955 (2003).
12. Unwin, N. Refined structure of the nicotinic acetylcholine receptor at 4 Å resolution. *J. Mol. Biol.* **346**, 967–989 (2005).
13. Brejc, K. *et al.* Crystal structure of an ACh-binding protein reveals the ligand-binding domain of nicotinic receptors. *Nature* **411**, 269–276 (2001).
14. Celie, P. H. *et al.* Nicotine and carbamylcholine binding to nicotinic acetylcholine receptors as studied in AChBP crystal structures. *Neuron* **41**, 907–914 (2004).
15. Hansen, S. B. *et al.* Structures of *Aplysia* AChBP complexes with nicotinic agonists and antagonists reveal distinctive binding interfaces and conformations. *EMBO J.* **24**, 3635–3646 (2005).
16. Dellisanti, C. D., Yao, Y., Stroud, J. C., Wang, Z. Z. & Chen, L. Crystal structure of the extracellular domain of nAChR α1 bound to α-bungarotoxin at 1.94 Å resolution. *Nature Neurosci.* **10**, 953–962 (2007).
17. Giraudat, J., Dennis, M., Heidmann, T., Chang, J. Y. & Changeux, J. P. Structure of the high-affinity binding site for noncompetitive blockers of the acetylcholine receptor: Serine-262 of the delta subunit is labeled by [^{3}H]chlorpromazine. *Proc. Natl Acad. Sci. USA* **83**, 2719–2723 (1986).
18. Blanton, M. P. & Cohen, J. B. Identifying the lipid-protein interface of the *Torpedo* nicotinic acetylcholine receptor: Secondary structure implications. *Biochemistry* **33**, 2859–2872 (1994).
19. Wilson, G. G. & Karlin, A. The location of the gate in the acetylcholine receptor channel. *Neuron* **20**, 1269–1281 (1998).
20. Cymes, G. D., Ni, Y. & Grosman, C. Probing ion-channel pores one proton at a time. *Nature* **438**, 975–980 (2005).
21. Wang, H. L., Cheng, X., Taylor, P., McCammon, J. A. & Sine, S. M. Control of cation permeation through the nicotinic receptor channel. *PLOS Comput. Biol.* **4**, e41 (2008).
22. Beckstein, O. & Sansom, M. S. The influence of geometry, surface character, and flexibility on the permeation of ions and water through biological pores. *Phys. Biol.* **1**, 42–52 (2004).
23. Harding, M. M. Metal-ligand geometry relevant to proteins and in proteins: Sodium and potassium. *Acta Crystallogr. D* **58**, 872–874 (2002).
24. Jha, A., Cadugan, D. J., Purohit, P. & Auerbach, A. Acetylcholine receptor gating at extracellular transmembrane domain interface: The cys-loop and M2–M3 linker. *J. Gen. Physiol.* **130**, 547–558 (2007).
25. Grutter, T. *et al.* Molecular tuning of fast gating in pentameric ligand-gated ion channels. *Proc. Natl Acad. Sci. USA* **102**, 18207–18212 (2005).
26. Lee, W. Y. & Sine, S. M. Principal pathway coupling agonist binding to channel gating in nicotinic receptors. *Nature* **438**, 243–247 (2005).
27. Lummis, S. C. *et al.* Cis-trans isomerization at a proline opens the pore of a neurotransmitter-gated ion channel. *Nature* **438**, 248–252 (2005).
28. Taly, A. *et al.* Normal mode analysis suggests a quaternary twist model for the nicotinic receptor gating mechanism. *Biophys. J.* **88**, 3954–3965 (2005).
29. Shimizu, H. *et al.* Global twisting motion of single molecular KcsA potassium channel upon gating. *Cell* **132**, 67–78 (2008).
30. Li, G. D. *et al.* Identification of a GABAA receptor anesthetic binding site at subunit interfaces by photolabeling with an etomidate analog. *J. Neurosci.* **26**, 11599–11605 (2006).

Supplementary Information is linked to the online version of the paper at www.nature.com/nature.

Acknowledgements We thank P. Koehl for his program Aquasol and help with electrostatic calculations; P. Delepelaire and S. Edelstein for discussions; the staff of ESRF (Grenoble) ID14 and ID23 beamlines for data collection; facilities of the Pasteur Institute (A. Haouz for crystallogenesis, P. England for ultracentrifugation experiments, J. d'Alayer for mass spectroscopy controls and J. Bellalou for help in protein expression); and B. De Foresta (CEA, Orsay) for a gift of the two brominated DDM analogues. The latter diffraction data sets were collected at SLS and PSI (Villingen, Switzerland). We thank M. Fuchs for assistance during data collection; and the IDRIS supercomputer centre and its support staff for allocating CPU time at very short notice (project 082292). This work was supported by the Région Ile-de-France (N.B.), the Association Française contre les Myopathies, the Collège de France (C.L.P.), the Commission of the European Communities (Neurocypres project; H.N.) and the Network of European Neuroscience Institutes (ENI-NET).

Author Information Coordinates of GLIC have been deposited in the Protein Data Bank under accession number 3eam.Reprints and permissions information is available at www.nature.com/reprints. Correspondence and requests for materials should be addressed to M.D. (marc.delarue@pasteur.fr) or P.-J.C. (pjcorrin@pasteur.fr).

©2008 Macmillan Publishers Limited. All rights reserved